Communication in Physical Sciences 2025, 12(4): 1352-1369

Enhancing $AgBiS_2$ Solar Cell Efficiency: Buffer Layer Comparison and Parameter Optimization

Muteeu A. Olopade* and Soko Swaray

Received: 12 February 2025/Accepted: 01 March 2025/Published: 08 March 2025
https://dx.doi.org/10.4314/cps.v12i4.16

Abstract: *This study endeavours to address the enhancement of the performance characteristics of $AgBiS_2$ solar cells through the introduction of CdS, CdZnS, and ZnS buffer layers, with and without an Sb_2S_3 back surface field (BSF), using SCAPS-1D simulation software. The findings indicate that CdZnS surpasses other buffer materials, achieving a maximum efficiency of 14.81% when integrated with the Back Surface Field (BSF). An optimal absorber thickness of 250 nm is identified, yielding an efficiency of 14.17%. The study further reveals that an increase in defect density adversely affects cell performance, with efficiency decreasing from 11.2% to 8.5% as defect density rises from 1.0×10^5 cm^{-3} to 1.0×10^{17} cm^{-3}. Temperature effects are evaluated, with CdZnS exhibiting exceptional thermal stability, maintaining high performance across a broad temperature range (280K to 400K). The influence of parasitic resistances is also examined, with efficiency values of 0.31%, 15.35%, and 10.05% recorded for CdS, CdZnS, and ZnS buffer layers, respectively, under varying shunt resistance conditions. The study emphasizes the advantageous properties of $AgBiS_2$, particularly its high absorption coefficient of approximately 10^5 cm^{-1} and suitable band gap of about 1.3 eV, underscoring its potential for photovoltaic applications. These findings offer valuable insights for optimizing $AgBiS_2$-based solar cells and suggest areas for future experimental validation.*

Key words: *Buffer layer, $AgBiS_2$, Defect density, Temperature, Photovoltaic.*

Muteeu Abayomi Olopade,
Department of Physics, University of Lagos, Nigeria
E-mail address: molopade@unilag.edu.ng
Orcid id: 0000-0002-1126-9027

Soko Swaray
Department of Physics, Fourah Bay College, University of Sierra Leone
E-mail address: sokoswaray264@gmail.com

1.0 Introduction

The utilization of solar energy for power generation is a viable strategy to ameliorate the global energy crisis. However, for power from the sun to be a feasible replacement to conventional energy sources, solar cell technology that converts energy from the sun into electricity must balance affordability and reliability (Sayeem et al., 2024). The technology of Crystalline silicon has significantly advanced, moving from laboratory research to commercial deployment. Crystalline silicon solar cells constitutes up to 90% of the global solar market (Baek et al., 2024). Cost efficiency is observed when material utilization is reduced and the energy conversion efficiency is increased. Thin-film solar cells (TFSCs) present a compelling option for electricity generation due to their high efficiency, low production costs, and substantial stability. These attributes render them a promising candidate for widespread adoption in the solar power market. These attributes establish them as viable alternatives to silicon-based photovoltaic (PV) systems (Guo et al., 2008). The conversion efficiency of amorphous silicon (a-Si) solar cells, a prevalent type of thin-film solar cell, is 14.0% (Kang, 2021). Silver bismuth sulfide ($AgBiS_2$) is a promising photoconductive material with intrinsically balanced durability among the non-toxic ternary chalcogenides that can be used in photovoltaics (Viñes et al., 2017). With a remarkable absorption coefficient of approximately 10^5 cm^{-1} and an appropriate band gap of about 1.3 eV (Wang et al., 2023). The $AgBiS_2$ absorber is a semiconductor material with distinct optoelectronic characteristics suitable for PV applications (Bernechea et al., 2016) . They were the first to report the utilization of $AgBiS_2$ Nanocrystal (NCs) as a solar cell material; however, reports of $AgBiS_2$ bulk and nanocrystal production date this considerably (Liang et al., 2015). $AgBiS_2$ NC-based solar cells fabricated at room pressure and below 100 °C demonstrated a certified PCE of 6.3%. Previous research has indicated that $AgBiS_2$ has the potential to enhance solar cell efficiency through various experimental methodologies. A solution-processed mixed ABS recently exhibited an efficiency of 7.3% (Burgués-Ceballos et al., 2022). For PV cells based on ABS, a theoretical investigation has reported a PCE of 26% (Akhil & Balakrishna, 2022). With a small active surface (0.06 cm^2), this device employed a vapor-assisted solution technique to achieve a power conversion efficiency (PCE) of 10.20% (X. Li et al., 2024). Moreover, the efficiency was 9.53% with a larger active surface of 1.00 cm^2 under standard global illumination conditions of 100 mW/cm^2 AM 1.5 (Kim et al., 2022). Despite the promising characteristics of $AgBiS_2$ perovskite solar cells, including their low manufacturing costs (Green, 2016), their application has been hindered by their low power conversion efficiency (PCE), poor stability, and low charge carrier mobility. Although SCAPS-1D has been extensively used to study the effects of interface defects and absorber thickness in various solar cell technologies, research specifically targeting these parameters in $AgBiS_2$-based solar cells is limited. This study seeks to address this gap by investigating how variations in the buffer layer affect the performance of $AgBiS_2$ solar cells using SCAPS-1D. This is accomplished by numerically simulating and analyzing $AgBiS_2$ solar cell device models using SCAPS-1D for three distinct buffer layers, CdS, CdsZns, ZnS, and with Sb_2S_3 as the Back Surface Field (BSF) for the three stated buffer materials, varying MoO_3 hole transport layer, absorber layer, absorber defect density, buffer layer thicknesses, operating temperatures, and parasitic resistance (Rs and Rsh). Voc, Jsc, FF (%), and eta (%) are the four essential solar cell performance parameters that were recorded and optimized.

2.0 Materials and Methods

Fig 1. Diagrammatic illustration of the solar cell structure utilized in this research: ITO, ZnO, CdS, CdZnS, ZnS, $AgBiS_2$, Sb_2S_3, Spiro-OMeTAD and MoO_3. The solar cell was subjected to testing at a temperature of 300 K, under a global air mass of AM1.5 G, with light exposure at an intensity of 100 mW/cm^2. In the device architecture, Spiro-OMeTAD serves as the hole transport layer (HTL), strategically positioned between the absorber layer and the metal electrode. This organic small molecule enhances efficient hole extraction and transport while inhibiting electron recombination at the interface. The incorporation of Spiro-OMeTAD is essential for achieving high power conversion efficiency and device stability. SCAPS-1D, a one-dimensional solar cell simulator developed by Burgelman et al., (Verschraegen & Burgelman, 2007), was used. This software was utilized to model the proposed solar cell structure and to evaluate its performance metrics. SCAPS-1D (Hima & Lakhdar, 2020; Pindolia et al., 2022) is instrumental for researchers in the field of solar cells, facilitating the analysis of device structures, particularly in terms of electrical properties and spectral responses. The parameters employed for thin-film solar cells in our numerical simulations are comprehensively detailed in Table 1, and the buffer layers' parameters are summarized in Table 2.

Poisson's equation, according to equation 1, elucidates the relationship between potential and space charges. The concentrations of free carriers, specifically electrons and holes, are represented by equations 2 and 3, respectively. The diffusion length, indicative of the carriers' transport capability within a solar cell, is contingent upon the diffusion coefficient and carrier lifetime, as illustrated in equation 4. The absorption coefficient, which quantifies the extent of energy absorption by a material, according to equation 5.

$$\varphi(x) = [n(x) - p(x) - N_D{+}(x) + N_A{-}(x) - pt(x) + nt(x)] \quad (1)$$

where φ is the electrostatic potential, n is the density of free electron, p is the density of free hole, N_D^+ is the ionized donor-like doping density, N_A^- is the ionized acceptor-like doping density, p_t is the trapped hole density, n_t is the trapped electron density.

$$n = N_c exp(E_f - \frac{E_c}{K_{BT}}) \quad (2)$$

$$p = N_v exp(E_v - \frac{E_f}{K_{BT}}) \quad (3)$$

Where, E_f is Fermi level, k_B is Boltzmann constant, T is temperature, E_c and E_v are energy levels under a steady state.

$$L = \sqrt{D\tau} \quad (4)$$

Where, L is diffusion length, **τ** is carrier lifetime.

$$\alpha(\lambda) = (A + \frac{B}{hv}) \sqrt{hv - E_{gap}} \quad (5)$$

where A and B are the absorption constants, h is Planck's constant, v is light speed.

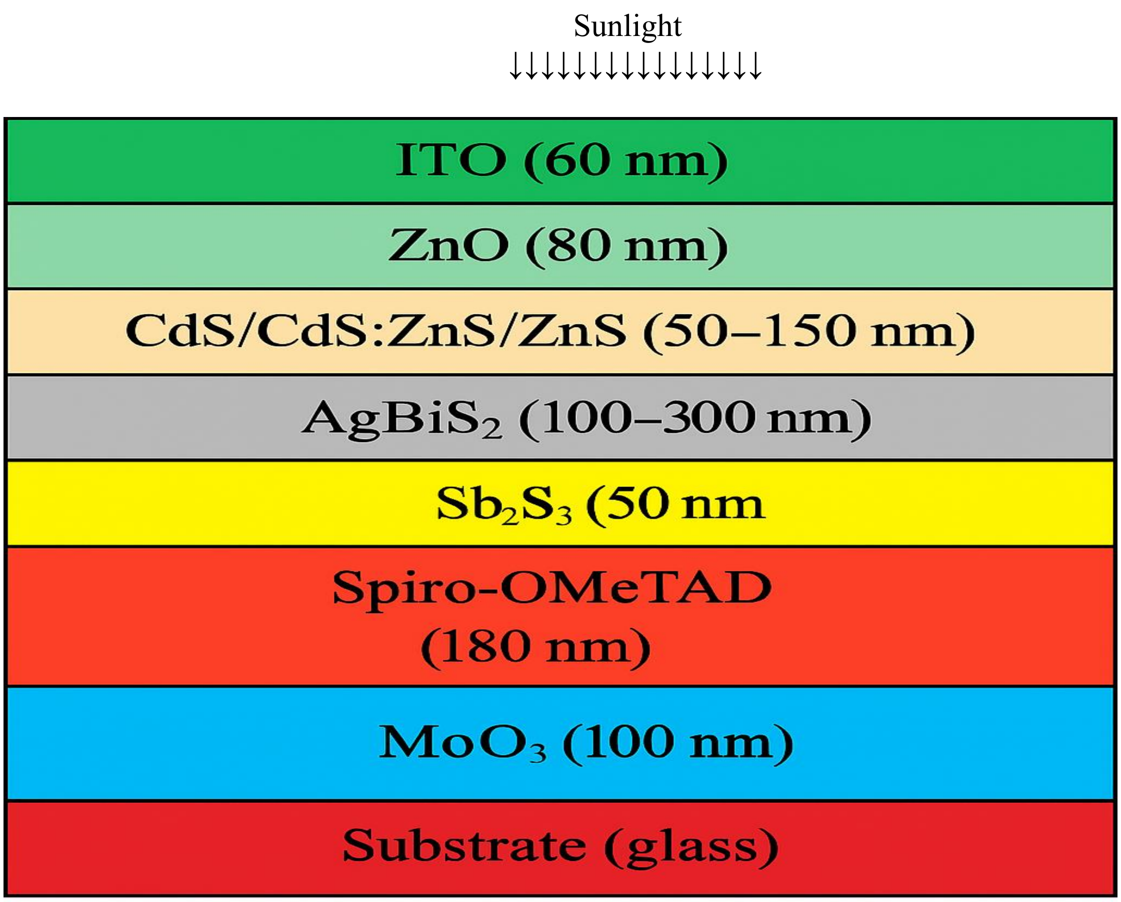

Fig. 1: A diagrammatic configuration of the $AgBiS_2$ thin-film solar cells ($ITO/ZnO/CdS/CdsZns/ZnS/AgBiS_2/Sb_2S_3$/Spiro-OMeTAD/$MoO_3$)

Table 1: Initial input numerical simulation parameters for the thin film solar cell (Ahamed et al.,)

Parameters	MoO$_3$	Spiro-OMeTAD	Sb$_2$S$_3$	AgBiS$_2$	ZnO	ITO
Thickness (nm)	100	180	50	100-300	80	60
Bandgap (Ev)	1.7	1.5	1.62	1.3	3.3	4.2
Electron affinity (Ev)	4.2	4.5	4.5	4.5	4.6	4.1
Dielectric permittivity	13.6	10	9	10	9	10
CB effective density of states (cm^{-3})	2.2×10^{18}	2.2×10^{18}	2.2×10^{18}	2.2×10^{18}	2.2×10^{18}	2.2×10^{18}
VB effective density of states (cm^{-3})	1.8×10^{19}	1.8×10^{19}	1.8×10^{19}	1.8×10^{19}	1.8×10^{19}	1.8×10^{19}
Electron thermal velocity (cms^{-1})	1×10^{7}	1×10^{7}	1×10^{7}	1×10^{7}	1×10^{7}	1×10^{7}
Hole thermal velocity (cms^{-1})	1×10^{7}	1×10^{7}	1×10^{7}	1×10^{7}	1×10^{7}	1×10^{7}
Electron mobility (cm^2/Vs)	100	100	98	100	100	50
Hole mobility (cm^2/Vs)	25	25	10	25	25	75
Shallow uniform donor density, ND (cm^{-3})	0	1×10^{1}	0	5×10^{15}	1×10^{18}	1×10^{19}
Shallow uniform acceptor density, Nu (cm^{-3})	1×10^{16}	2×10^{14}	1×10^{16}	1×10^{1}	0	0
Defect type	-	Donor	-	Acceptor	-	-
Defect density (cm^{-3})	-	1×10^{13}	-	1×10^{16}	-	-

Table 2: Present input parameters for the different buffer materials *(Jhuma et al., 2019)*

Parameter	CdS	CdSZnS	ZnS
Thickness (nm)	50–150	50–150	50–150
Bandgap (eV)	2.4	2.98	3.5
Electron affinity (eV)	4.5	4.2	4.5
Dielectric permittivity	10	9.4	1.8×10^{18}
CB effective density of states (cm^{-3})	2.2×10^{18}	2.2×10^{18}	1.8×10^{19}
VB effective density of states (cm^{-3})	1.8×10^{19}	1.8×10^{19}	1×10^{7}
Electron thermal velocity (cm/s)	1×10^{7}	1×10^{7}	1×10^{7}
Hole thermal velocity (cm/s)	1×10^{7}	1×10^{7}	1×10^{7}
Electron mobility (cm^2/Vs)	100	270	100
Hole mobility (cm^2/Vs)	25	27	25
Shallow uniform donor density, ND (cm^{-3})	1.8×10^{18}	5×10^{17}	5×10^{15}
Shallow uniform acceptor density, NA (cm^{-3})	0	0	1×10^{1}
Defect type	–	–	–
Defect density (cm^{-3})	–	–	–

3.0 Results and Discussion

$AgBiS_2$, known for its high absorption coefficient and band gap, shows great promise for photovoltaic applications. The proposed solar cell design, ITO/$AgBiS_2$/Spiro-OMeTAD/MoO_3, exhibits excellent performance across various parameters. CdZnS, when paired with an Sb_2S_3 back surface field, surpasses other buffer materials, achieving an impressive efficiency of 14.81%. The optimal absorber thickness is set at 250 nm, and CdZnS consistently maintains high performance across different temperatures.

3.1 Impact of MoO_3 Hole Transport Layer Thickness

The study explores the optimization of the MoO_3 hole transport layer (HTL) thickness to improve the photovoltaic (PV) performance of solar cells. By adjusting the thickness from 100 nm to 150 nm, the research evaluates how key photovoltaic parameters affect short-circuit current density (Jsc), open-circuit voltage (Voc), fill factor (FF), and efficiency (η), as shown in Fig. 2. Initially, the open-circuit voltage (Voc) rises with increasing thickness, reaching a maximum at about 120 nm, before decreasing with further thickness increases. Voc is influenced by the energy alignment at the interface between the active layer and the HTL. A well-designed HTL optimizes energy band alignment, promoting efficient hole extraction. For MoO_3 layers thinner than 120 nm, incomplete film formation may occur, leading to higher leakage current and inefficient hole extraction (Horejs et al., 2017). The ideal thickness for a solar cell's thin film (HTL) is around 120 nm, which reduces recombination and enhances the built-in electric field. If HTLs are too thin, they can cause increased series resistance, lowering Voc and short-circuit current density (Jsc). Thin HTLs have lower series resistance, allowing efficient charge extraction and maintaining a high fill factor (FF). As the MoO_3 layer becomes thicker, series resistance increases, reducing FF and Voc. Thin HTLs optimize Voc, while thicker layers may impede light absorption, decreasing efficiency. Achieving the right HTL thickness is essential for balancing charge extraction, minimizing resistive losses, and reducing recombination. The interaction of these factors results in an optimal thickness of approximately 120 nm, where Voc and η are maximized, achieving an efficiency of 11.68%.

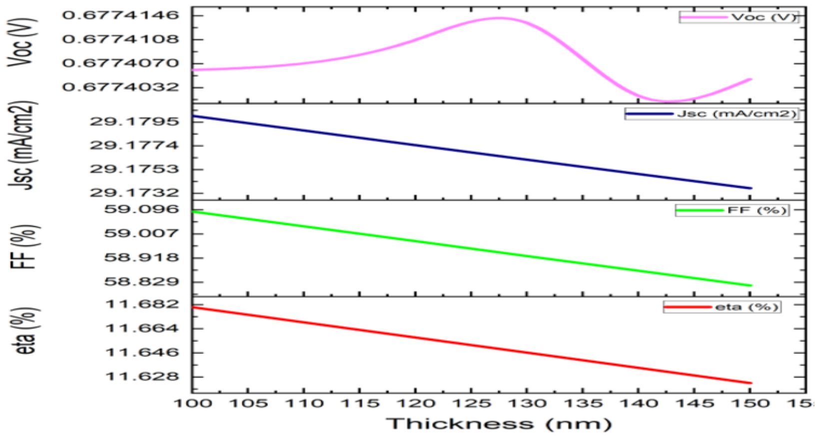

Fig 2. Effect of MoO_3 hole transport layer (HTL) thickness on the photovoltaic (PV) performance

3.2 Impact of $AgBiS_2$ Absorber Layer Thickness on Device Performance

The thickness of the absorber layer significantly impacts device characteristics (Chang et al., 2019), making it a crucial parameter in solar cell engineering. As the primary site for electron-hole pair formation, the absorber layer shows improved incident light absorption and pair generation with increased thickness (Schwartz et al., 2020). When designing the device architecture, special focus was placed on the absorber layer's thickness, a crucial factor affecting both optical and electronic performance. A thickness of 250 nm was chosen for the absorber, informed by prior research suggesting that ultra-thin $AgBiS_2$ layers within the 250–300 nm range achieve an ideal balance between light absorption and charge carrier extraction. This thickness is adequate to capture a substantial portion of the incident light spectrum while remaining thin enough to enable efficient carrier transport and collection. By avoiding excessive thickness, recombination losses are reduced, thereby enhancing the device's overall efficiency. A slight increase in the open-circuit voltage (Voc) was observed as the absorber thickness grew, indicating enhanced charge carrier generation (Abdelaziz et al., 2020). Voc progresses almost linearly from about 0.69 V at 300 nm. The short-circuit current density (Jsc) generally increased with thickness, though with some fluctuations, reaching around 35.81 mA/cm² at a thickness of 250 nm before slightly decreasing at 260 nm. This pattern suggests improved light absorption and carrier collection up to a certain thickness (Tan et al., 2016). The fill factor (FF) was approximately 57.46% at 60 and gradually declined as the thickness increased to 300 nm, possibly due to higher series resistance or recombination losses in thicker layers. The efficiency (η) showed stability with minor fluctuations, peaking at 14.17% at 250 nm thickness as shown in Fig. 3. This represents the optimal balance between absorption and recombination effects, as η depends on Voc, Jsc, and FF. Below 250 nm, Jsc decreases due to reduced absorption; beyond this, Jsc stabilizes while FF declines sharply. Although Voc increased slightly beyond 250 nm, FF decreased significantly (57.2%). Beyond 250 nm, efficiency decreases due to resistive and recombination losses. Thus, 250 nm emerges as the optimal thickness for effective absorption and maximum efficiency.

3.3 Impact of $AgBiS_2$ Absorber Defect Density on Photovoltaic Metrics

To evaluate the influence of intrinsic material quality on device performance, we conducted simulations on $AgBiS_2$-based solar cells, investigating a broad range of defect densities from (1×10^5 – 1×10^{17} cm^3). This comprehensive range allows us to include both high-quality films with minimal trap states and lower-quality materials where defect-mediated recombination is pronounced. By systematically varying the defect density, we can assess the impact of non-radiative recombination on key photovoltaic parameters, including open-circuit voltage (Voc), fill factor (FF), and the overall efficiency of the device.

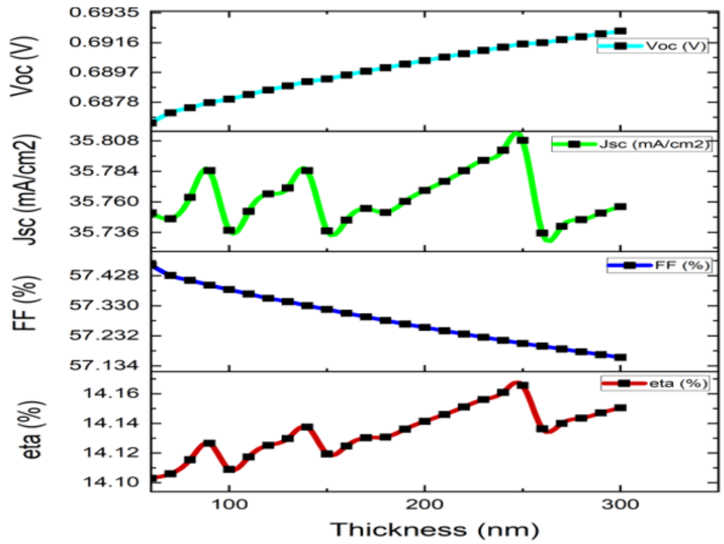

Fig. 3 presents plots of the absorber thickness vs. the key photovoltaic parameters.

These defects facilitate nonradiative recombination of photogenerated electron-hole pairs, thereby impeding electricity generation (Ju et al., 2020). Defects act as traps for carriers, reducing their lifetime and diffusion length, which limits charge transport to electrodes and increases recombination losses. The defect density ranged from Nt=1.0×10^{5} cm^{-3} to Nt=1.0×10^{17} cm^{-3}. This ultimately results in decreased photovoltage and power conversion efficiency. To achieve high efficiency in $AgBiS_2$-based solar cells, advanced processing techniques and defect-passivation strategies are employed (Zou et al., 2024). The simulation outcomes further reveal a marked reduction in performance with the escalation of defect density. Notably, the short-circuit current density (Jsc) diminishes from 29.1 mA/cm² at Nt = 0 cm^{-3} to 28.1 mA/cm² at Nt = 1.0×10^{17} cm^{-3}, as a result of charge carriers recombining before contributing to the photocurrent. In parallel, the open-circuit voltage (Voc) declines from 0.676 V to 0.650 V, attributed to the proliferation of non-radiative recombination pathways. The fill factor (FF) also experiences a decrease from 61.0% to 56.5%, which is linked to the increased series resistance due to defect-induced carrier trapping. Consequently, the overall power conversion efficiency (η) falls from 11.2% to 8.5%. These observations align with the findings emphasizing the imperative to minimize defect density (Nt) through meticulous material engineering and optimized fabrication processes, as illustrated in Fig. 4.

3.4 Effect of CdS, CdZnS, and ZnS buffer layer thicknesses without (BSF)

The simulation utilized a constant absorber layer thickness of 300 nm, while the buffer layer thicknesses varied from 50 to 150 nm. Optimizing the CdS layer thickness is essential for balancing light transmission, surface coverage, and electrical characteristics (Chouhan et al., 2018). The wide bandgap of CdS permits the transmission of most of the visible spectrum of sunlight, thereby minimizing parasitic absorption and ensuring optimal light penetration to the solar cell's active layer (Chen et al., 2024).

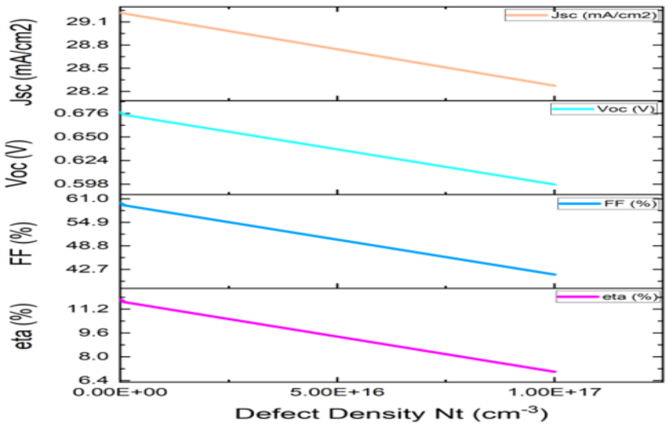

Fig 4. Illustrate a plot of $AgBiS_2$ Absorber Defect Density vs Perovskite metrics: eta (%), FF (%), Jsc and Voc

The CdS bandgap aligns with the absorber (Krishnakumar et al., 2009) and TCO layers, facilitating efficient separation of photogenerated charge carriers, allowing electrons to migrate into CdS while holes remain in the absorber (Keshav & Mahesha, 2021). The CdS configuration enhances device performance by minimizing conduction band offset, reducing electron transport barriers (Çetinkaya et al., 2022), carrier recombination, and improving transparency, while also influencing light scattering and absorption (Tashkandi & Sampath, 2011). Thinner layers enhance light penetration but may compromise surface coverage (Shockley & Queisser, 1961), whereas thicker CdS layers reduce light transmission and resistance, impacting efficiency and achieving a minimum efficiency of 1.08% as shown in Fig. 5a. The buffer layer plays a crucial role in forming p-n junctions and improving charge carrier transport in solar cells (Po et al., 2011). Fig. 5b demonstrates the influence of CdZnS buffer layer thickness on four key parameters, highlighting its advantageous properties in enhancing the buffer layer (Xu et al., 2017), compatibility with the absorber layer (Elumalai & Uddin, 2016). The buffer layer in CdZnS semiconductors optimizes band alignment, minimizes recombination, and maximizes fill factor, achieving the highest efficiency of 11.88% at 70 nm (Madelung, 2004). The open-circuit voltage (Voc) increased gradually with ZnS thickness, reaching a significant peak beyond 140 nm, as shown in Fig. 5c. ZnS improves outdoor solar durability by reducing surface recombination velocities, improving charge carrier lifetime and efficiency, and facilitating charge screening due to its higher dielectric constant (Huang et al., 2016). Thicker ZnS buffers reduce defect density and improve electric field uniformity (Bhattarai et al., 2022). An efficiency (eta) of approximately 10.37% was achieved by optimizing ZnS thickness to 50 nm.

3.5 Effect of (CdS, CdZnS, and ZnS) buffer layer thicknesses with Sb_2S_3 as (BSF)

Antimony sulfide (Sb_2S_3) shows potential for thin-film solar cells as a back-surface field (BSF). Sb_2S_3 consists of the abundant elements antimony and sulfur (Eensalu et al., 2023). The BSF layer improves solar cell performance by collecting photogenerated carriers and reducing recombination at the back contact. Sb_2S_3 prevents minority carriers from reaching the back contact, reducing surface recombination and increasing open-circuit voltage (Voc) (Liu et al., 2024) It creates an electric field directing minority carriers toward the junction, enhancing charge collection efficiency (Younsi et al., 2024; Zhao et al., 2021). It also reflects unabsorbed photons to the absorber layer, increasing efficiency (Guo et al., 2008).

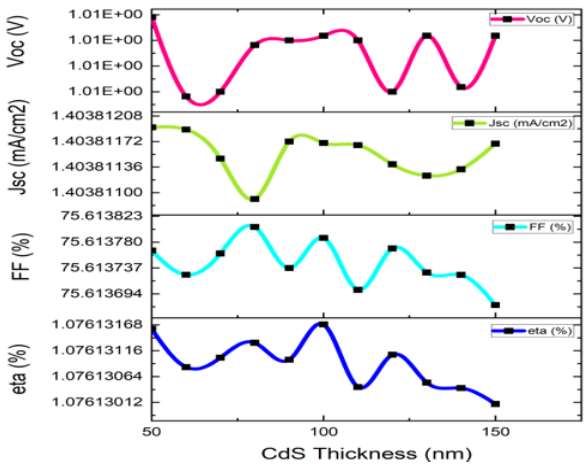

Fig. 5a

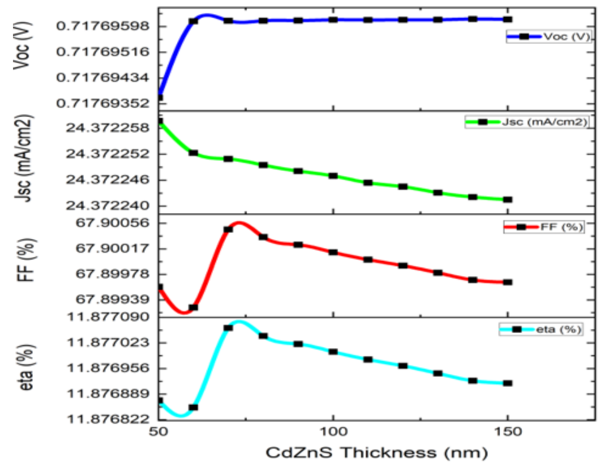

Fig. 5b

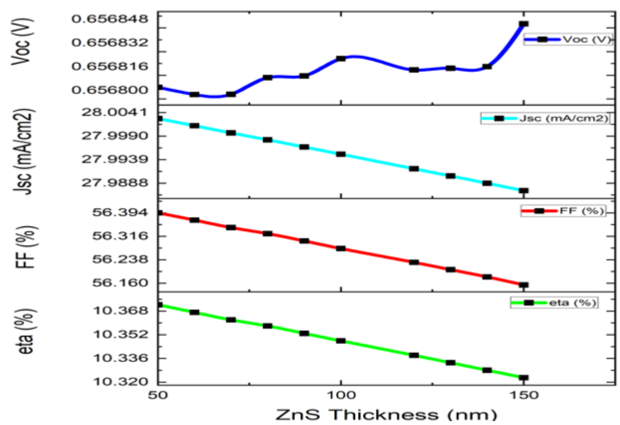

Fig. 5c

Figs. 5a-c shows the effect of different buffer thickness layers (CdS, CdZnS, and ZnS) on key photovoltaic performance parameters without BSF

The simulation used a constant absorber layer thickness of 300 nm, while buffer layer thicknesses varied between 50 and 150 nm with Sb_2S_3 as the BSF for each buffer layer, as depicted in Figs. 6a, 6b, and 6c. The study investigates the role of the CdS buffer layer in improving solar cell efficiency, highlighting its role in light transmission, charge carrier collection, carrier lifetime, current generation, and photon absorption (Amin et al., 2010). Thicker CdS layers increase optical absorption, but their bandgap (~2.4 eV) (Granata et al., 1996) reduces photocurrent generation. CdS thickness affects fill factor (FF) and efficiency, with thicker layers increasing series resistance (Groehn et al., 2016). CdZnS minimizes optical absorption and promotes electron transfer, while Sb_2S_3 improves charge collection. CdZnS optimizes band alignment (Wu et al., 2013) With efficiency peaking at 50 nm (Elborg et al., 2015). ZnS and Sb_2S_3 improve efficiency by reducing interface recombination and enhancing junction quality (Hernández-Calderón et al., 2020). Thicker ZnS layers cause higher losses, while thinner layers improve photon penetration. The efficiencies for CdS, CdZnS, and ZnS buffer layers were 0.24%, 14.81%, and 10.37%, respectively.

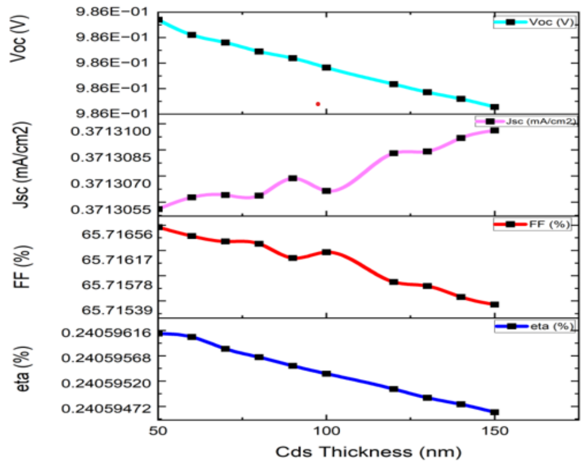

Fig. 6a

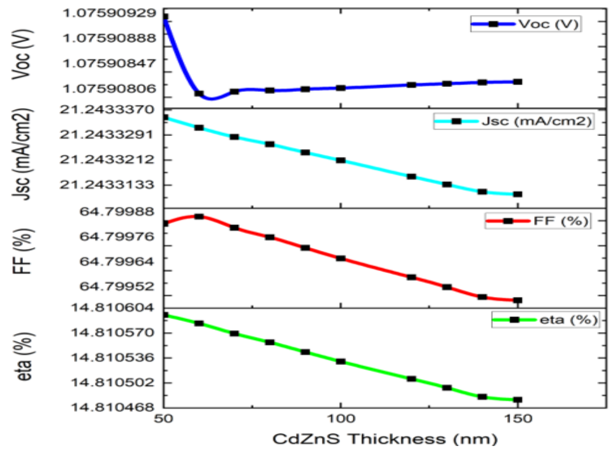

Fig. 6b

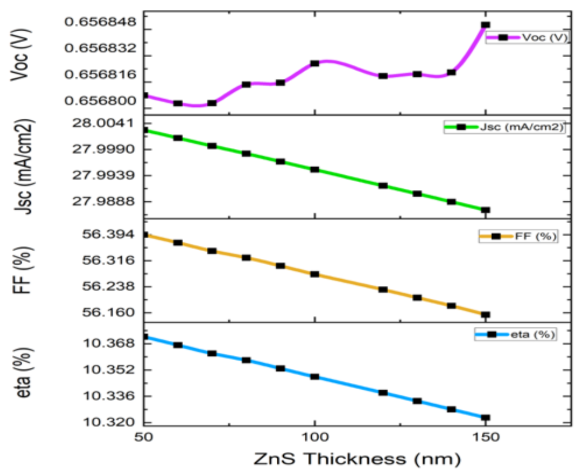

Fig. 6c

Figs. 6a-c show the effects of varying the thickness of different buffer layers (CdS, CdZnS, and ZnS) on key photovoltaic performance parameters with BSF.

3.6 Impact of variation of working temperature for the different Buffer materials (CdS, CdZnS, and ZnS).

Temperature is a critical factor influencing the performance of photovoltaic (PV) systems (Maiello et al., 2013). This study examines the impact of temperature on these systems by simulating conditions ranging from 280 K to 400 K under 1 Sun illumination (100 mW cm-2, AM1.5G spectrum). Absolutely, and exploring that 280–400 K range is particularly insightful because it captures both the lower operational limit—say, during early morning hours or overcast days—and the upper bounds experienced under full sun and limited airflow. You might also consider coupling this thermal range with humidity variation or light intensity fluctuations to mimic more complex real-world stressors. Fig. 7a depicts the efficiency (η) as a function of temperature for CdS, CdZnS, and ZnS. The efficiency of CdS remains consistently low at approximately 0.31% across the temperature spectrum. In contrast, CdZnS begins with a high efficiency of 17.25% and exhibits an increase from 300 K to approximately 380 K, indicating robust thermal stability. ZnS experiences an efficiency increase to 10.48% at 310 K before declining, suggesting thermal instability. Efficiency is influenced by open-circuit voltage (Voc), short-circuit current (Jsc), and fill factor (FF). Elevated temperatures result in a decrease in

Voc due to recombination losses, while Jsc may increase owing to enhanced carrier mobility (Löper et al., 2012). Initially, ZnS demonstrates an increase in FF, followed by a sharp decline, whereas CdZnS maintains a stable FF. Regarding Jsc, ZnS achieves the highest values, and CdZnS exhibits thermal stability in both Jsc and Voc. The Voc of ZnS decreases at elevated temperatures. Fig. 7b illustrates that the FF of CdS and ZnS increases with temperature, but ZnS declines due to thermal degradation. Fig.7c indicates that CdS and CdZnS maintain steady Jsc, while ZnS achieves higher values but with reduced efficiency. Fig. 7d shows CdS with low Voc, CdZnS with stability, and ZnS with a decline, indicating thermal instability (H. X. Li, 2012). CdZnS is more suitable for high-temperature applications, while ZnS performs optimally only at lower temperatures.

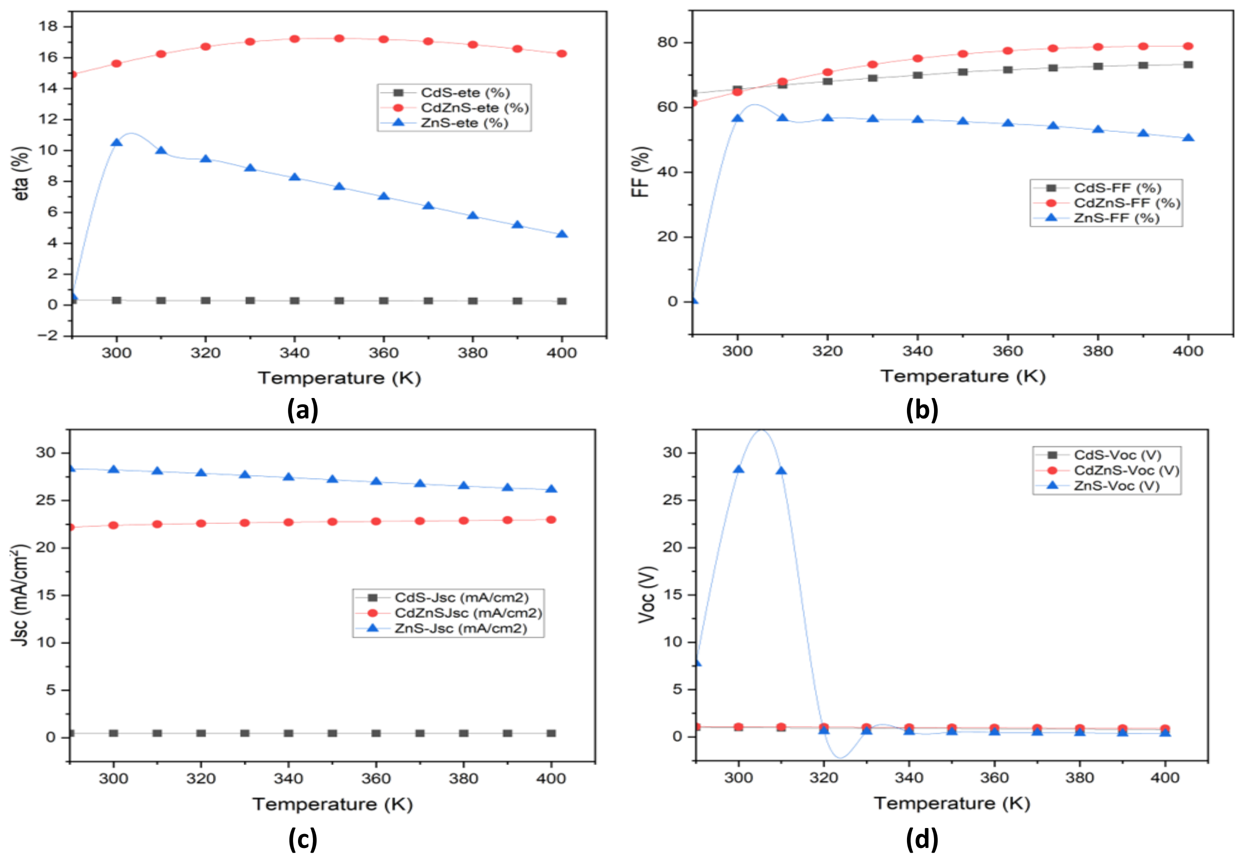

Fig. (7a)-(d) depict how Temperature impacts photovoltaic performance parameters

3.7 Effect of Shunt Resistance (R_{sh}) on Device Operation

To clarify how parasitic resistances affect device performance, we examine the impact of altering R_{sh} from 10000 cm² to 100000 cm². Shunt resistance is indicative of the degree of leakage current pathways across the device, typically resulting from defects, pinholes, or edge shunting. A high R_{sh} value, ranging from 10000 Ω.cm² to 100000 Ω.cm², is preferred and was selected for ideal and near-ideal scenarios to represent minimal leakage and high device integrity. Lower R_{sh} values were incorporated to simulate scenarios prone to defects or degradation effects over time. The selected range encompasses the anticipated performance window of fabricated devices and facilitates reliability and tolerance analysis. Figs. 8a-d illustrate how shunt resistance (R_{sh}) influences key photovoltaic (PV) parameters: short-circuit current density (Jsc), open-circuit voltage (Voc), fill factor (FF), and conversion efficiency (η) in solar cells with various buffer layers (CdS, CdZnS, and ZnS). R_{sh} represents unintended current paths within the solar cell, allowing current to bypass the load and flow directly between terminals. In an ideal cell, R_{sh} approaches infinity, indicating minimal leakage current (Dhass et al., 2012). Parasitic currents from finite R_{sh} values can reduce cell performance. While Jsc remains constant, Voc increases with higher R_{sh}, which decreases leakage currents. A greater R_{sh} improves the fill factor (FF) by reducing resistive losses, thereby enhancing the maximum power point and overall cell efficiency (Upadhyay & Singh, 2023). Efficiency, calculated as the product of Voc, Jsc, and FF normalized by input power, primarily improves due to increases in Voc and FF as R_{sh} rises, given the relative stability of Jsc.

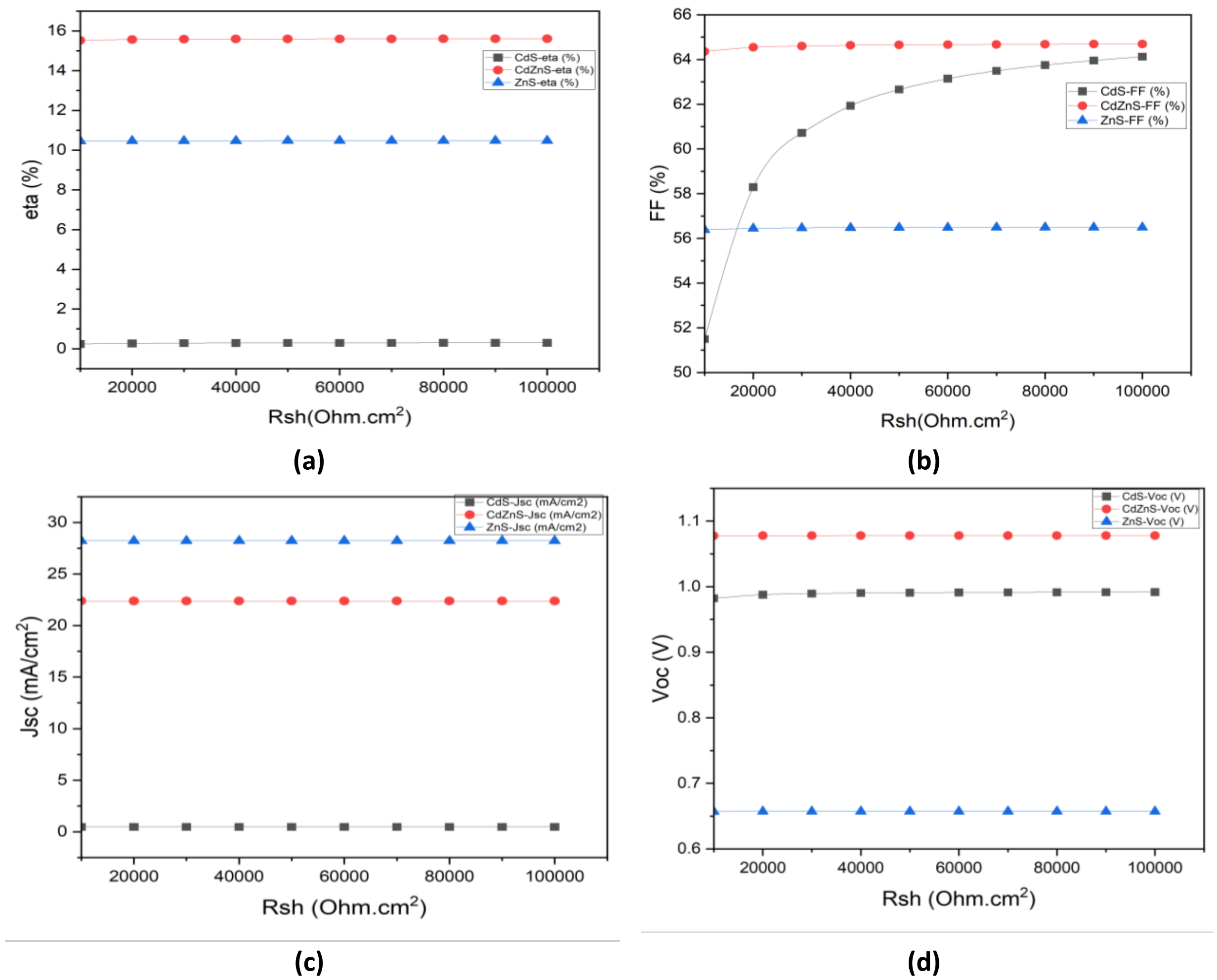

Figs. 8a-d show the influence of Shunt Resistance on key photovoltaic performance metrics- eta (%), FF (%), (Jsc) and (Voc)

The buffer layers exhibit unique characteristics: CdS shows oscillatory Jsc behavior, possibly due to interference effects or recombination phenomena at the buffer/absorber interface. CdZnS demonstrates improved Voc and FF compared to CdS, suggesting reduced recombination and better carrier transport. ZnS shows the most significant R_{sh}-dependent efficiency, indicating its ability to minimize leakage paths and enhance carrier selectivity, resulting in superior performance at high R_{sh} values. In summary, increasing R_{sh} reduces leakage current losses, leading to improved FF and efficiency while maintaining relatively constant Jsc. The choice of buffer layer significantly influences these trends due to variations in material properties, with CdZnS showing the greatest potential for high-efficiency solar cells. The efficiencies obtained for the different buffer materials (CdS, CdZnS, and ZnS) are 0.31%, 15.35%, and 10.05%, respectively.

3.8 Effect of Series Resistance (R_s) on Device Operation

The series resistance is composed of contributions from the bulk material, the contact resistance at the electrodes, and the sheet resistance of transparent conductive layers. In this simulation, ideal values of 10000 Ω.cm² to 100000 Ω.cm² were chosen to signify efficient charge extraction with minimal resistive losses. Figs 9a-d demonstrate the impact of series resistance (R_s) on the performance of solar cells. Series resistance (R_s) is a pivotal factor in determining the efficiency of solar cells, as it restricts the flow of current and leads to resistive losses. An increase in R_s can result in slight variations in the open-circuit voltage (Voc) for materials such as CdS and CdZnS, whereas its effect on ZnS is minimal.

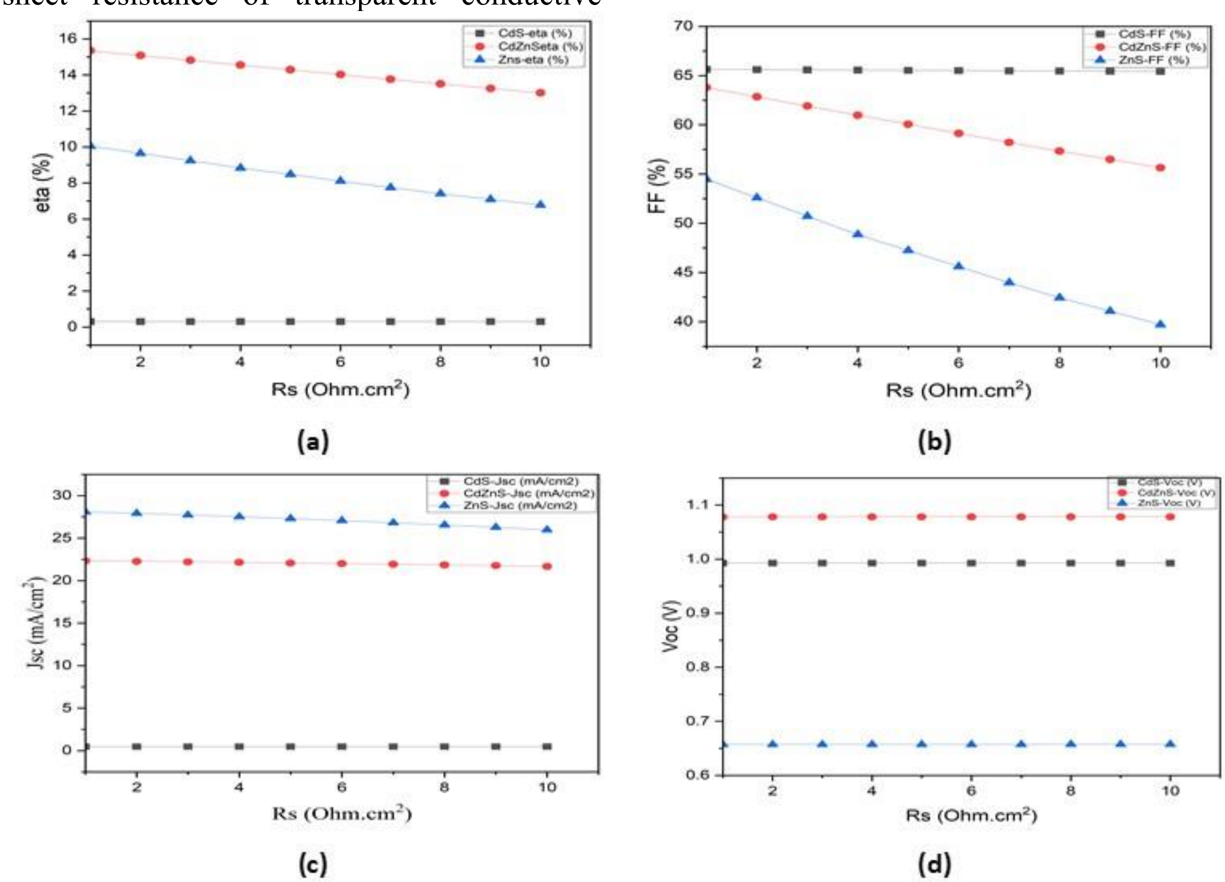

Figs. 9a-d depict the effect of series resistance (Rs) on device performance parameters, including eta (%), FF (%), (Jsc), and (Voc).

The short-circuit current density (Jsc) remains constant for CdS and CdZnS but decreases significantly for ZnS as R_s increases, due to ZnS's lower conductivity and mobility compared to the other materials. As R_s rises, the fill factor (FF) also diminishes because of voltage drops at the maximum power point (Prakash et al., 2018), ultimately reducing overall efficiency. CdS and CdZnS exhibit a slight increase in Voc, while ZnS experiences a notable reduction in both Jsc and efficiency. To enhance solar cell performance, it is essential to reduce R_s by improving layer conductivity and optimizing material quality. The influence of R_s is more pronounced in materials with higher intrinsic resistance, such as ZnS, compared to those with superior conductive properties, like CdS and CdZnS. Minimizing R_s is crucial for optimizing solar cell performance, particularly for materials like ZnS that are more susceptible to resistive losses. Strategies to mitigate R_s include enhancing layer conductivity, optimizing contact interfaces, and utilizing higher-quality materials with lower intrinsic resistance. The efficiencies recorded for CdS, CdZnS, and ZnS are 0.31%, 10.05%, and 15.35%, respectively.

4.0 Conclusion

The study investigates $AgBiS_2$ thin-film solar cells using numerical simulations. It finds promising characteristics like a high absorption coefficient and band gap, making it viable for photovoltaic applications. CdZnS outperforms other buffer materials, achieving 14.81% efficiency with a back surface field. The optimal absorber thickness is 250 nm, and CdZnS exhibits the best thermal stability. However, further research is needed, including experimental validation and comparison with other solar cell technologies.

Acknowledgement

We appreciate Prof. Marc Burgelman and his team of the University of Ghent for providing the SCAPS-1D software to execute this research.

5.0 References

Abdelaziz, S., Zekry, A., Shaker, A., & Abouelatta, M. (2020). Investigating the performance of formamidinium tin-based perovskite solar cell by SCAPS device simulation. *Optical Materials*, *101*, 109738. https://doi.org/10.1016/j.optmat.2020.109738

Ahamed, T., Rahman, A., Rahaman, I., Mamun, A., Shiam, I. F., Hasan, M., Ahammed, T., Karmakar, S., Parash, H. H., & Ghosh, S. (n.d.). *Numerical investigation of optimal buffer layer and performance evaluation on CdTe solar cell*.

Akhil, S., & Balakrishna, R. G. (2022). AgBiS$_2$ as a photoabsorber for eco-friendly solar cells: A review. *Journal of Materials Chemistry A*, 10,16, pp. 8615–8625. https://doi.org/10.1039/D2TA00549B

Amin, N., Matin, M. A., Aliyu, M. M., Alghoul, M. A., Karim, M. R., & Sopian, K. (2010). Prospects of Back Surface Field Effect in Ultra-Thin High-Efficiency CdS/CdTe Solar Cells from Numerical Modeling. *International Journal of Photoenergy*, *2010*, pp.1–8. https://doi.org/10.1155/2010/578580

Baek, S., Lee, G., Kim, H. R., Im, S., Kim, C., & Joo, J. H. (2024). Novel approach to enhancing layered double hydroxide catalyst performance and stability through substrate structure control. *Chemical Engineering Journal*, *496*, 154295. https://doi.org/10.1016/j.cej.2024.154295

Bernechea, M., Cates, N., Xercavins, G., So, D., Stavrinadis, A., & Konstantatos, G. (2016). Solution-processed solar cells based on environmentally friendly AgBiS$_2$ nanocrystals. *Nature Photonics*, 10,8, pp. 521–525. https://doi.org/10.1038/nphoton.2016.108

Bhattarai, S., Pandey, R., Madan, J., Ahmed, F., & Shabnam, S. (2022). Performance improvement approach of all inorganic perovskite solar cell with numerical simulation. *Materials Today Communications*, *33*, 104364. https://doi.org/10.1016/j.mtcomm.2022.104364

Burgués-Ceballos, I., Wang, Y., & Konstantatos, G. (2022). Mixed AgBiS$_2$ nanocrystals for photovoltaics and photodetectors. *Nanoscale*, 14,13, pp. 4987–4993. https://doi.org/10.1039/D2NR00589A

Çetinkaya, Ç., Çokduygulular, E., Kınacı, B., Güzelçimen, F., Özen, Y., Sönmez, N. A., & Özçelik, S. (2022). Highly improved light harvesting and photovoltaic performance in CdTe solar cell with functional designed 1D-photonic crystal via light management engineering. *Scientific Reports*, 12, 1, 11245. https://doi.org/10.1038/s41598-022-15078-w

Chang, W., Tian, H., Fang, G., Guo, D., Wang, Z., & Zhao, K. (2019). Simulation of innovative high efficiency perovskite solar cell with Bi-HTL: NiO and Si thin films. *Solar Energy*, 186, pp. 323–327. https://doi.org/10.1016/j.solener.2019.05.017

Chen, S., Ye, Y., Ishaq, M., Ren, D., Luo, P., Wu, K., Zeng, Y., Zheng, Z., Su, Z., & Liang, G. (2024). Simultaneous Band Alignment Modulation and Carrier Dynamics Optimization Enable Highest Efficiency in Cd-Free Sb_2Se_3 Solar Cells. *Advanced Functional Materials*, 34,40, 2403934. https://doi.org/10.1002/adfm.202403934

Chouhan, A. S., Jasti, N. P., & Avasthi, S. (2018). Effect of interface defect density on performance of perovskite solar cell: Correlation of simulation and experiment. *Materials Letters*, *221*, pp. 150–153. https://doi.org/10.1016/j.matlet.2018.03.095

Dhass, A. D., Natarajan, E., & Ponnusamy, L. (2012). Influence of shunt resistance on the performance of solar photovoltaic cell. In *2012 International Conference on Emerging Trends in Electrical Engineering and Energy Management (ICETEEEM)* (pp. 382–386). https://doi.org/10.1109/ICETEEEM.2012.6494522

Eensalu, J. S., Mandati, S., Don, C. H., Finch, H., Dhanak, V. R., Major, J. D., Grzibovskis, R., Tamm, A., Ritslaid, P., Josepson, R., Käämbre, T., Vembris, A., Spalatu, N., Krunks, M., & Oja Acik, I. (2023). Sb_2S_3 Thin-Film Solar Cells Fabricated from an Antimony Ethyl Xanthate Based Precursor in Air. *ACS Applied Materials & Interfaces*, 15,36, pp. 42622–42636. https://doi.org/10.1021/acsami.3c08547

Elborg, M., Noda, T., Mano, T., Jo, M., Sakuma, Y., Sakoda, K., & Han, L. (2015). Voltage dependence of two-step photocurrent generation in quantum dot intermediate band solar cells. *Solar Energy Materials and Solar Cells*, 134, pp. 108–113. https://doi.org/10.1016/j.solmat.2014.11.038

Elumalai, N. K., & Uddin, A. (2016). Open circuit voltage of organic solar cells: An in-depth review. *Energy & Environmental Science*, 9,2, pp. 391–410. https://doi.org/10.1039/C5EE02871J

Granata, J. E., Sites, J. R., Contreras-Puente, G., & Compaan, A. D. (1996). Effect of CdS thickness on CdS/CdTe quantum efficiency [solar cells]. In *Conference Record of the Twenty Fifth IEEE Photovoltaic Specialists Conference - 1996* (pp. 853–856). https://doi.org/10.1109/PVSC.1996.564262

Green, M. A. (2016). Commercial progress and challenges for photovoltaics. *Nature Energy*, 1,1, 15015. https://doi.org/10.1038/nenergy.2015.15

Groehn, A. J., Lewandowski, A., Yang, R., & Weimer, A. W. (2016). Hybrid radiation modeling for multi-phase solar-thermal reactor systems operated at high-temperature. *Solar Energy*, 140, pp.130–140. https://doi.org/10.1016/j.solener.2016.11.003

Guo, Q., Kim, S. J., Kar, M., Shafarman, W. N., Birkmire, R. W., Stach, E. A., Agrawal, R., & Hillhouse, H. W. (2008). Development of $CuInSe_2$ Nanocrystal and Nanoring Inks for Low-Cost Solar Cells. *Nano Letters*, 8,9, pp. 2982–2987. https://doi.org/10.1021/nl802042g

Hernández-Calderón, V., Vigil-Galán, O., Guc, M., Carrillo-Osuna, A., Ramírez-Velasco, S., Sánchez-Rodríguez, F. J., Vidal-Fuentes, P., Giraldo, S., Saucedo, E., & Sánchez, Y. (2020). CdS/ZnS Bilayer Thin Films Used As Buffer Layer in 10%-Efficient Cu$_2ZnSnSe_4$ Solar Cells. *ACS Applied Energy Materials*, 3,7, pp. 6815–6823. https://doi.org/10.1021/acsaem.0c00937

Hima, A., & Lakhdar, N. (2020). Enhancement of efficiency and stability of CH$_3NH_3GeI_3$ solar cells with CuSbS$_2$. *Optical Materials*, *99*, 109607. https://doi.org/10.1016/j.optmat.2019.109607

Horejs, C.-M., St-Pierre, J.-P., Ojala, J. R. M., Steele, J. A. M., Da Silva, P. B., Rynne-Vidal, A., Maynard, S. A., Hansel, C. S., Rodríguez-Fernández, C., Mazo, M. M., You, A. Y. F., Wang, A. J., Von Erlach, T., Tryggvason, K., López-Cabrera, M., & Stevens, M. M. (2017). Preventing tissue fibrosis by local biomaterials interfacing of specific cryptic extracellular matrix information. *Nature Communications*, 8,1, 15509. https://doi.org/10.1038/ncomms15509

Huang, F., Zhang, Q., Xu, B., Hou, J., Wang, Y., Massé, R. C., Peng, S., Liu, J., & Cao, G. (2016). A comparison of ZnS and ZnSe passivation layers on CdS/CdSe co-sensitized quantum dot solar cells. *Journal of Materials Chemistry A*, 4,38, pp. 14773–14780. https://doi.org/10.1039/C6TA01590E

Jhuma, F. A., Shaily, M. Z., & Rashid, M. J. (2019). Towards high-efficiency CZTS solar cell through buffer layer optimization. *Materials for Renewable and Sustainable Energy*, 8,1, 6. https://doi.org/10.1007/s40243-019-0144-1

Ju, M.-G., Dai, J., Ma, L., Zhou, Y., & Zeng, X. C. (2020). AgBiS$_2$ as a low-cost and eco-friendly all-inorganic photovoltaic material: Nanoscale morphology–property relationship. *Nanoscale Advances*, 2(,2, pp. 770–776. https://doi.org/10.1039/C9NA00505F

Kang, H. (2021). Crystalline Silicon vs. Amorphous Silicon: The Significance of Structural Differences in Photovoltaic Applications. *IOP Conference Series: Earth and Environmental Science*, *726,1*, 012001. https://doi.org/10.1088/1755-1315/726/1/012001

Keshav, R., & Mahesha, M. G. (2021). Investigation on performance of CdTe solar cells with CdS and bilayer ZnS / CdS windows grown by thermal evaporation technique. *International Journal of Energy Research*, 45, 5, pp. 7421–7435. https://doi.org/10.1002/er.6325

Kim, C., Kozakci, I., Kim, J., Lee, S. Y., & Lee, J. (2022). Highly Efficient (>9%) Lead-Free AgBiS$_2$ Colloidal Nanocrystal/Organic Hybrid Solar Cells. *Advanced Energy Materials*, *12*(25), 2200262. https://doi.org/10.1002/aenm.202200262

Krishnakumar, V., Ramamurthi, K., Klein, A., & Jaegermann, W. (2009). Band alignment of differently treated TCO/CdS interface. *Thin Solid Films*, 517, 7, pp. 2558–2561. https://doi.org/10.1016/j.tsf.2008.11.065

Li, H. X. (2012). Kinematic Shakedown Analysis of Anisotropic Heterogeneous Materials: A Homogenization Approach. *Journal of Applied Mechanics*, *79,4*, 041016. https://doi.org/10.1115/1.4006056

Li, X., Yu, H., Ma, X., Liu, Z., Huang, J., Shen, Y., & Wang, M. (2024). Thin film AgBiS$_2$ solar cells with over 10 % power conversion efficiency enabled by vapor-assisted solution process treatment. *Chemical Engineering Journal*, 495, 153328. https://doi.org/10.1016/j.cej.2024.153328

Liang, N., Chen, W., Dai, F., Wu, X., Zhang, W., Li, Z., Shen, J., Huang, S., He, Q., Zai, J., Fang, N., & Qian, X. (2015). Homogenously hexagonal prismatic $AgBiS_2$ nanocrystals: Controlled synthesis and application in quantum dot-sensitized solar cells. *CrystEngComm*, 17,9, pp. 1902–1905. https://doi.org/10.1039/C4CE02405B

Liu, X., Cai, Z., Wan, L., Xiao, P., Che, B., Yang, J., Niu, H., Wang, H., Zhu, J., Huang, Y., Zhu, H., Zelewski, S. J., Chen, T., Hoye, R. L. Z., & Zhou, R. (2024). Grain Engineering of Sb_2S_3 Thin Films to Enable Efficient Planar Solar Cells with High Open-Circuit Voltage. *Advanced Materials*, 36, 1, 2305841. https://doi.org/10.1002/adma.202305841

Löper, P., Pysch, D., Richter, A., Hermle, M., Janz, S., Zacharias, M., & Glunz, S. W. (2012). Analysis of the Temperature Dependence of the Open-Circuit Voltage. *Energy Procedia*, 27, pp.135–142. https://doi.org/10.1016/j.egypro.2012.07.041

Madelung, O. (2004). *Semiconductors: Data Handbook*. Springer Berlin Heidelberg. https://doi.org/10.1007/978-3-642-18865-7

Maiello, P., Zoppi, G., Miles, R. W., Pearsall, N., & Forbes, I. (2013). Chalcogenisation of Cu–Sb metallic precursors into $Cu_3Sb(Se_xS_{1-x})_3$. *Solar Energy Materials and Solar Cells*, 113, pp. 186–194. https://doi.org/10.1016/j.solmat.2013.02.016

Pindolia, G., Shinde, S. M., & Jha, P. K. (2022). Optimization of an inorganic lead free $RbGeI_3$ based perovskite solar cell by SCAPS-1D simulation. *Solar Energy*, 236, pp. 802–821. https://doi.org/10.1016/j.solener.2022.03.053

Po, R., Carbonera, C., Bernardi, A., & Camaioni, N. (2011). The role of buffer layers in polymer solar cells. *Energy Environ. Sci.*, *4*(2), 285–310. https://doi.org/10.1039/C0EE00273A

Prakash, M. B., Sai, R. P., & Reddy, K. S. (2018). *Understanding the effect of series resistance for solar PV module*. 6(2).

Sayeem, S. A., Siddika, Mst. A., Basu, S. R., Mondal, B. K., & Hossain, J. (2024). Numerical Expedition on the Potential of $AgBiS_2$-Based Thin Film Solar Cells Employing Different Carrier Transport Layers. *ACS Omega*, 9,33, pp.35490–35502. https://doi.org/10.1021/acsomega.4c02375

Schwartz, D., Murshed, R., Larson, H., Usprung, B., Soltanmohamad, S., Pandey, R., Barnard, E. S., Rockett, A., Hartmann, T., Castelli, I. E., & Bansal, S. (2020). Air Stable, High-Efficiency, Pt-Based Halide Perovskite Solar Cells with Long Carrier Lifetimes. *Physica Status Solidi (RRL) – Rapid Research Letters*, 14, 8, 2000182. https://doi.org/10.1002/pssr.202000182

Shockley, W., & Queisser, H. J. (1961). Detailed Balance Limit of Efficiency of p-n Junction Solar Cells. *Journal of Applied Physics*, 32, 3, pp. 510–519. https://doi.org/10.1063/1.1736034

Tan, K., Lin, P., Wang, G., Liu, Y., Xu, Z., & Lin, Y. (2016). Controllable design of solid-state perovskite solar cells by SCAPS device simulation. *Solid-State Electronics*, 126, pp. 75–80. https://doi.org/10.1016/j.sse.2016.09.012

Tashkandi, M. A., & Sampath, W. S. (2011). Morphology of CdS thin films: Pinholes and their effect on open circuit voltage in CdS/CdTe solar cells. In *2011 37th IEEE Photovoltaic Specialists Conference* (pp. 001700–001704). https://doi.org/10.1109/PVSC.2011.6186282

Upadhyay, S., & Singh, D. (2023). Effect of series and shunt resistance on the performance of Kesterite solar cells. *International Journal of Scientific Research in Modern Science and*

Technology, *2,8*, *pp.* 38–45. https://doi.org/10.59828/ijsrmst.v2i8.134

Verschraegen, J., & Burgelman, M. (2007). Numerical modeling of intra-band tunneling for heterojunction solar cells in scaps. *Thin Solid Films*, 515, 15, pp. 6276–6279. https://doi.org/10.1016/j.tsf.2006.12.049

Viñes, F., Konstantatos, G., & Illas, F. (2017). Bandgap engineering by cationic disorder: Case study on AgBiS$_2$. *Phys. Chem. Chem. Phys.*, 19, 41, pp. 27940–27944. https://doi.org/10.1039/C7CP05118B

Wang, W., Gao, C., Chen, Y., Shen, T., Dong, M., Yao, B., & Zhu, Y. (2023). Cubic AgBiS$_2$ Powder Prepared Using a Facile Reflux Method for Photocatalytic Degradation of Dyes. *Micromachines*, 14, 12, 2211. https://doi.org/10.3390/mi14122211

Wu, T., Mayaffre, H., Krämer, S., Horvatić, M., Berthier, C., Kuhns, P. L., Reyes, A. P., Liang, R., Hardy, W. N., Bonn, D. A., & Julien, M.-H. (2013). Emergence of charge order from the vortex state of a high-temperature superconductor. *Nature Communications*, 4, 1, 2113. https://doi.org/10.1038/ncomms3113

Xu, X.-B., Wang, X.-Y., Gu, W.-P., Quan, S., & Zhang, Z. (2017). Study on influences of CdZnS buffer layer on CdTe solar cells. *Superlattices and Microstructures*, *109*, 463–469. https://doi.org/10.1016/j.spmi.2017.05.033

Younsi, Z., Meddour, F., Bencherif, H., Hossain, M. K., Marasamy, L., Sasikumar, P., Revathy, M. S., Ghotekar, S., Karim, M. R., Ayyar, M., Haldhar, R., & Rubel, M. H. K. (2024). Scrutinizing transport phenomena and recombination mechanisms in thin film Sb$_2S_3$ solar cells. *Scientific Reports*, 14, 1, 12460. https://doi.org/10.1038/s41598-024-56041-1

Zhao, R., Yang, X., Shi, H., & Du, M.-H. (2021). Intrinsic and complex defect engineering of quasi-one-dimensional ribbons Sb$_2S_3$ for photovoltaics performance. *Physical Review Materials*, *5,5*, 054605. https://doi.org/10.1103/PhysRevMaterials.5.054605

Zou, B., Chen, D., Qammar, M., Ding, P., Ko, P. K., Wu, W., Shivarudraiah, S. B., Yan, H., & Halpert, J. E. (2024). In Situ Surface Metal Passivation on AgBiS$_2$ Nanocrystals for Trap-Reduced Inverted Solar Cells. *ACS Applied Energy Materials*, 7,19, pp. 8271–8277. https://doi.org/10.1021/acsaem.4c01307.

Declaration

Consent for publication

Not applicable

Availability of data

Data shall be made available on demand.

Competing interests

The authors declared no conflict of interest

Ethical Consideration

Not applicable

Funding

There is no source of external funding.

Authors' Contributions

The authors declare that the article was jointly written by the authors for the publication of this paper.